



Pergamon

Available online at www.sciencedirect.com

SCIENCE @ DIRECT®

Acta Materialia 51 (2003) 1359–1372



www.actamat-journals.com

Effect of phase fraction on the tri-junction in two-phase nanoparticle systems

J.M. Howe^{*}, A.M. Mebed¹, K. Chatterjee, P. Li, M. Murayama²,
W.C. Johnson

Department of Materials Science and Engineering, University of Virginia, 116 Engineers Way, Charlottesville, VA 22904-4745, USA

Received 3 October 2002; received in revised form 1 November 2002; accepted 5 November 2002

Abstract

The equilibrium dihedral angles at the solid–solid–vapor tri-junctions of two-phase Cu–Ag alloy nanoparticles 40–100 nm in diameter were measured as a function of phase fraction using transmission electron microscopy. The {111} solid–solid interface was cusp-oriented while the surface orientations of the Cu-rich and Ag-rich phases at the tri-junction were mostly free to vary. The dihedral angles at the tri-junction were found to vary with the phase fraction, due to the coupling between the relative amounts of each phase and the equilibrium conditions at the tri-junction. This equilibrium condition was used to measure the ratio of the Ag-rich and Cu-rich surface energies to the {111} interfacial energy, which were found as 2.1 and 3.5, respectively.

© 2003 Acta Materialia Inc. Published by Elsevier Science Ltd. All rights reserved.

Keywords: Transmission electron microscopy; Interfaces; Surface energy; Phase transformations; Nanoparticles

1. Introduction

It is well known that the balance among the surface and interfacial energy densities determines the resulting equilibrium dihedral angles at a three-phase junction (or tri-junction) [1–5]. This situation is illustrated in Fig. 1 for the case of two

solid phases (α and β) in contact with their vapor (v) and applies, for example, both to grain (α/α) and to interphase (α/β) boundary grooves. For an isotropic system, in which the interfacial energy density is independent of the interface normal, thermodynamic equilibrium at the three-phase or tri-junction yields two independent conditions:

$$\frac{\sigma_{\alpha\beta}}{\sin \theta_v} = \frac{\sigma_{\alpha v}}{\sin \theta_\beta} = \frac{\sigma_{\beta v}}{\sin \theta_\alpha}, \quad (1)$$

where σ and θ are the indicated surface/interfacial energy densities and dihedral angles among the α , β and v phases, respectively. Since $\theta_\alpha + \theta_\beta + \theta_v = 2\pi$, there exist three conditions that uniquely

^{*} Corresponding author. Tel.: +1-434-982-5646; fax: +1-434-982-5660.

E-mail address: jh9s@virginia.edu (J.M. Howe).

¹ On leave from Physics Department, Assuit University, Assuit 71516, Egypt.

² On leave from National Institute for Materials Science, Tsukuba, 305-0047, Japan.

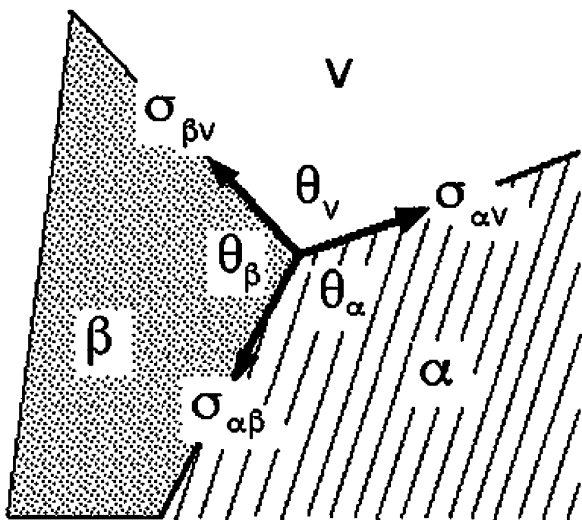


Fig. 1. A representative tri-junction with equilibrium dihedral angles θ and interfacial/surface energies σ between the α , β and v phases indicated.

determine the three dihedral angles of the tri-junction.

In an anisotropic system, the interfacial energy density depends on the interface normal and, in some cases, cusps and grooves in the plot of the interfacial energy can occur for certain crystallographic directions [1,5]. The dependence of the interfacial energy on interface orientation gives rise to torque terms that act on the tri-junction. The conditions for thermodynamic equilibrium applicable to a three-phase junction comprising anisotropic interfaces are of the form:

$$\sigma_{\alpha\beta} + \sigma_{\alpha v} \cos \theta_{\alpha} + \sigma_{\beta v} \cos \theta_{\beta} + \frac{\partial \sigma_{\alpha v}}{\partial \theta_{\alpha}} \sin \theta_{\alpha} + \frac{\partial \sigma_{\beta v}}{\partial \theta_{\beta}} \sin \theta_{\beta} = 0 \quad (2)$$

and

$$\sigma_{\beta v} + \sigma_{\alpha\beta} \cos \theta_{\beta} + \sigma_{\alpha v} \cos \theta_{\alpha} + \frac{\partial \sigma_{\alpha\beta}}{\partial \theta_{\beta}} \sin \theta_{\beta} + \frac{\partial \sigma_{\alpha v}}{\partial \theta_{\alpha}} \sin \theta_{\alpha} = 0, \quad (3)$$

where it is assumed that all interface normals are removed from any cusp orientation. Eqs. (2) and (3) were initially derived by Herring [1]. As for the isotropic system, these two conditions are sufficient to determine uniquely the dihedral angles of

the three-phase junction. In the limit of interfacial isotropy, the torque terms vanish and Eq. (2) simplifies to

$$\sigma_{\alpha\beta} + \sigma_{\alpha v} \cos \theta_{\alpha} + \sigma_{\beta v} \cos \theta_{\beta} = 0. \quad (4)$$

Eq. (4) is Young's equation [2], commonly used in the evaluation of wetting experiments [3–5]. It can be obtained directly from Eq. (1), using trigonometric arguments. In practice, the dihedral angles at a tri-junction are measured experimentally and then used to determine the grain boundary or interfacial energy, given known values for the surface energies of the phases.

The dihedral angles need not be uniquely determined when one of the interfaces is cusp-oriented. Hoffman and Cahn [6,7] showed that the force balance at the tri-junction giving rise to the equalities of Eqs. (2) and (3), is replaced by an inequality which eliminates one of the constraints on the dihedral angles. As a result, it should be possible for an equilibrium three-phase junction in which one interface is cusp-oriented to exhibit a range of dihedral angles. This situation has been discussed in detail recently with respect to grain boundaries [8].

In recent transmission electron microscope (TEM) investigations of two-phase Ag–Cu alloy nanoparticles, we observed large variations in the particle shapes and corresponding three-phase junction angles that appear consistent with the surface/interfacial-energy balance predictions of Hoffman and Cahn [6]. In particular, the observed dihedral angles appeared to depend on the relative phase-fractions of the Cu-rich and Ag-rich phases. In this paper, we present experimental observations and simple analytical calculations which show that the balance among the surface and interfacial energy densities at a three-phase junction and the resulting dihedral angles depend on the relative phase fractions of the solid phases. This result has particularly important implications in nanostructured materials, where phase volumes are small and particles are often able to obtain their equilibrium shape. It also presents a new method to determine the relative values of the surface and interfacial energy densities in two-phase systems, based on the variation of the dihedral angles at the three-phase junction with phase fraction.

2. Sample preparation and transmission electron microscopy

The alloy particles used in this study were formed by thermal evaporation of high-purity Ag and Cu metals from separate tungsten baskets onto heated (520 °C) amorphous-carbon TEM grids under high-vacuum (4×10^{-8} Torr) conditions [9]. After evaporation, the grids were held at 520 °C for 2 h to equilibrate and were then cooled to room temperature in vacuum. The samples were immediately transferred to the TEM for examination and/or stored under vacuum until observation.

Bright-field (BF) images and selected-area diffraction patterns (SADPs) of the Ag–Cu particles were obtained in a JEOL 2000FXII TEM operating at 200 kV, and high-resolution TEM (HRTEM) images of the particles were obtained in a JEOL 4000EX microscope operating at 400 kV, near Scherzer defocus (−48.5 nm). Energy-dispersive X-ray spectroscopy (EDXS) was performed in a JEOL 2010F field-emission gun TEM at 200 kV (employing both TEM 5–3 and CBD 0.5–9 modes) using an Oxford ultrathin-window detector and pulse processor, connected to a 4-pi Analysis board and Macintosh computer running the NIST Desktop Spectrum Analyzer (DTSA v. 2.5.1) program. Quantification of the X-ray spectra was performed by inputting the counts from DTSA into the Thin-Film Analysis program [10], using a calculated k -factor of 0.24 for the ratio of the Cu to Ag K_{α} X-ray peaks. All TEM analyses were performed using standard procedures [11].

The dihedral angles at the three-phase junctions were determined by digitizing TEM negatives of individual particles, drawing tangents to the tri-junctions by eye on the computer images, and measuring the resulting angles using Adobe Photoshop™ software. This process was repeated several times for each tri-junction and the average value of the angles was used, with a typical error of several degrees. In order to determine the relative values of the surface and interfacial energies, a line was best-fit to a plot of $\cos \theta_{\alpha}$ versus $\cos \theta_{\beta}$, using an orthogonal distance regression analysis [12]. This analysis minimizes the errors for $\cos \theta_{\alpha}$ and $\cos \theta_{\beta}$, both of which are independent variables and subject to measurement error. The projected

area fractions of the α and β phases in the two-phase particles were measured from the digital images, using a routine in NIH Image software.

3. Equilibrium particle shape and dihedral angles

In this section, the equations specifying the equilibrium shape of a two-phase crystalline system in contact with its vapor and the corresponding boundary conditions for the equilibrium angles at a tri-junction containing an interface with a fixed orientation are obtained as a function of the relative amounts of each phase using variational calculus. The two solid–vapor surface energy densities ($\sigma_{\alpha v}$, $\sigma_{\beta v}$) are assumed to be isotropic while the solid–solid interface is assumed to be cusp-oriented with interfacial energy density $\sigma_{\alpha\beta}$. Interfacial and surface-stress effects are neglected and the composition fields within each phase are assumed homogeneous. These conditions imply that the phase compositions are independent of particle size and alloy composition, and that the effect of segregation on the surface and interfacial energies is ignored. The equilibrium shape of the two-phase particle is that which minimizes the sum of the surface and interfacial energies for a given phase fraction of the two solid phases. It is assumed that the experimental system is sufficiently small that global equilibrium has been obtained.

Initially, a two-dimensional α – β – v system is considered, as depicted in Fig. 2. The Ag-rich and Cu-rich phases are designated as α and β , respectively. In keeping with TEM images showing the α/β interface to be planar and coincident with the $\{111\}$ plane, the α/β interface is constrained to lie along the y -axis. The x -axis is taken to be a mirror plane requiring the derivative y' to become undefined as $x \rightarrow a^+$ and $x \rightarrow b^-$, where a and b are the particle dimensions along the x -axis. With the assumption of global equilibrium, the morphology of each phase depends on the amounts of each phase present. If A_{α} and A_{β} represent the areas of the α and β phases, respectively, then the following two constraints apply:

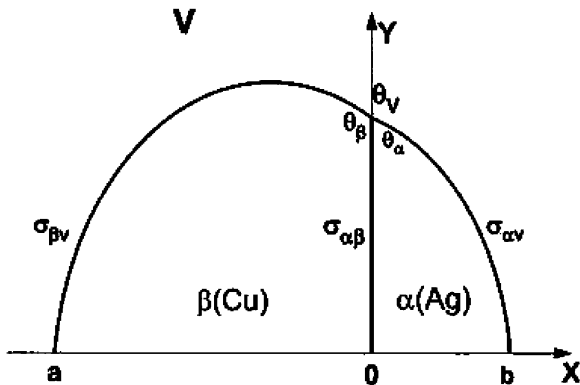


Fig. 2. Coordinate system and cross section of an equilibrium two-phase particle showing the Ag-rich (α), Cu-rich (β) and vapor (v) phases. The α/β interface is cusp-oriented and constrained to lie along the y -axis.

$$A_\alpha = \int_0^b y(x) dx \quad \text{and} \quad A_\beta = \int_a^0 y(x) dx. \quad (5)$$

Associating the Lagrange multipliers λ_α and λ_β with the two expressions of Eq. (5), the equilibrium shape is determined by minimizing the sum of the surface and interfacial energies, E^* :

$$E^* = \int_a^0 \{ \sigma_{\beta v} \sqrt{1 + (y')^2} - \lambda_\beta y \} dx + \sigma_{\alpha\beta} y(0) \quad (6)$$

$$+ \int_0^b \{ \sigma_{\alpha v} \sqrt{1 + (y')^2} - \lambda_\alpha y \} dx.$$

Recognizing that $y(x)$ is continuous on $[a, b]$, that $y'(x)$ can be discontinuous at $x = 0$, and that the functional is explicitly independent of x , yields the following Euler–Lagrange equations for the equilibrium particle shapes:

$$\lambda_\beta y - \frac{\sigma_{\beta v}}{\sqrt{1 + (y')^2}} = C_1, \quad x \in [a, 0] \quad (7)$$

and

$$\lambda_\alpha y - \frac{\sigma_{\alpha v}}{\sqrt{1 + (y')^2}} = C_2, \quad x \in [0, b], \quad (8)$$

where C_1 and C_2 are constants of integration. In

addition, there arises the natural boundary condition at the tri-junction:

$$\frac{\sigma_{\beta v} y'_-}{\sqrt{1 + (y'_-)^2}} - \frac{\sigma_{\alpha v} y'_+}{\sqrt{1 + (y'_+)^2}} + \sigma_{\alpha\beta} = 0 \quad \text{at } x = 0, \quad (9)$$

where

$$y'_- = \lim_{x \rightarrow 0^-} \frac{dy}{dx} \quad \text{and} \quad y'_+ = \lim_{x \rightarrow 0^+} \frac{dy}{dx}. \quad (10)$$

The following relationships then obtain from Fig. 2:

$$\frac{y'_-}{\sqrt{1 + (y'_-)^2}} = \cos \theta_\beta \quad \text{and} \quad \frac{-y'_+}{\sqrt{1 + (y'_+)^2}} = \cos \theta_\alpha. \quad (11)$$

Substituting these expressions into Eq. (9) yields:

$$\cos \theta_\beta = -\frac{\sigma_{\alpha\beta}}{\sigma_{\beta v}} - \frac{\sigma_{\alpha v}}{\sigma_{\beta v}} \cos \theta_\alpha, \quad (12)$$

which is just a rearrangement of Young's equation, Eq. (4), expressed such that the $\cos \theta_\beta$ varies directly with $\cos \theta_\alpha$, with the proportionality $-\sigma_{\alpha\beta}/\sigma_{\beta v}$.

The solution to Eqs. (7) and (8) is obtained as follows. Recognizing that $C_1 = 0$ and $C_2 = 0$ in order to satisfy the boundary conditions at $x = a$ and $x = b$, respectively, yields the following expression for y' on the domain $[0, b]$:

$$y' = \pm \sqrt{(\sigma_{\alpha v}/\lambda_\alpha y)^2 - 1}, \quad x \in [0, b], \quad (13)$$

where the correct sign must be determined. Integration of Eq. (13) yields:

$$(x + C_3)^2 + y^2 = \left(\frac{\sigma_{\alpha v}}{\lambda_\alpha} \right)^2, \quad x \in [0, b], \quad (14)$$

where C_3 is a constant of integration. Eq. (14) represents a circle that is truncated along the y -axis. The center of the circle is located at $(-C_3, 0)$ and has a radius $R_\alpha = \sigma_{\alpha v}/\lambda_\alpha$. A similar expression obtains for the β phase. The equilibrium shape of the two-phase system therefore consists of two truncated circles of radii R_α and R_β centered on the x -axis.

A similar analysis can be performed for a three-dimensional, two-phase system with the α/β interface lying along the y - z plane, assuming that the x -axis is an axis of rotation. In this case the equilibrium shape of each phase is a truncated sphere with its center located on the x -axis, and the equilibrium condition obtained at the tri-junction is the same as Eq. (12). The actual shape assumed by the two-phase system is not a truncated sphere owing to the presence of the substrate. However, as the particle shapes obtained at equilibrium consist of portions of a sphere and the boundary condition at the tri-junction, Eq. (12) remains valid. In the calculations presented here, the equilibrium shape of each particle is assumed to be a truncated sphere.

Other than the condition on the continuity of the particle shape, Eq. (12) is the only equilibrium condition at the tri-junction. As such, the dihedral angles are not uniquely determined at equilibrium, but depend on the shapes taken by the two phases and, hence, on their relative phase fractions. We measured $\cos \theta_\alpha$ and $\cos \theta_\beta$ experimentally as a function of the projected area fractions, to obtain the ratios of the energy densities, $\sigma_{\alpha\beta}/\sigma_{\beta\nu}$ and $\sigma_{\alpha\nu}/\sigma_{\beta\nu}$, using Eq. (12).

4. Transmission electron microscopy

4.1. BF imaging and selected-area diffraction

The Ag–Cu system was selected for study because it is a model eutectic alloy between two face-centered cubic (fcc) phases, each having limited solubility for the other [14]. Fig. 3 shows a BF TEM image and corresponding SADP of the evaporated Ag–Cu particles on the amorphous-carbon grid. Since the atomic number of Ag, 47, is nearly twice that of Cu, 29, the Ag-rich α phase usually appears darker than the Cu-rich β phase, except when the β phase is strongly diffracting and the α phase is not. Thus, it is often possible to distinguish the two phases based on their contrast in a BF image, particularly when the interface between them is nearly parallel to the electron beam. This is the case for the particles labeled A and B in Fig. 3(a), where the Ag-rich α phase appears darker. Most of the larger particles on the

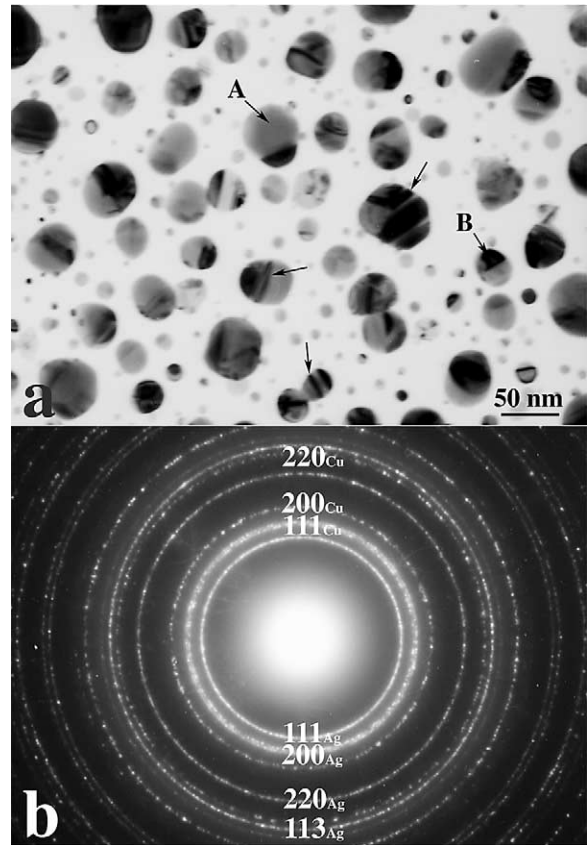


Fig. 3. (a) BF TEM image and (b) corresponding SADP of evaporated Ag–Cu nanoparticles on an amorphous-carbon grid.

grid consisted of two phases separated by one or more nearly planar interfaces (as for particles A and B) and both of the phases often contained stacking faults and/or twins, as indicated by arrows in several particles in Fig. 3(a). These defects always occurred on {111} planes in the phases, as is typical for fcc materials [15]. The two-phase particles had a random orientation on the carbon support so that particles with α/β interfaces parallel to the electron beam required for analysis (as for particle A in Fig. 3(a)), were found by viewing many particles. Many of the smaller particles on the grid were single-phase; they were usually nearly pure Ag, but occasionally they were almost pure Cu. The formation of this mixture of single and two-phase particles is likely due to the different condensation rates of the two metals on the substrate during evaporation, which leads to incomplete

alloying [16,17]. The two-phase particles that were used for the following diffraction, EDXS, and tri-junction measurements had diameters of 40–100 nm.

Both SAD and EDXS were used to confirm that the particles consisted of two distinct phases ($\alpha + \beta$) across the interface. The SADP in Fig. 3(b), taken using a large SAD aperture with many two-phase particles in the aperture, shows the presence of two superimposed fcc ring-patterns, one from the Ag-rich α phase and the other from the Cu-rich β phase, as labeled in the figure. The relative difference in lattice parameters between the two phases, $(a_\alpha - a_\beta)/a_\beta$, was measured using the well-separated $\{220\}$ rings in the patterns (the $\{111\}$ Cu and $\{200\}$ Ag rings nearly overlap) and yielded a value of $12.9 \pm 0.2\%$, which is essentially the same as the calculated value of 13.0% based on the lattice parameters of pure Ag (0.40857 nm) and pure Cu (0.36147 nm) [14,18], within the error of experimental measurement.

Fig. 4 shows a BF TEM image and correctly oriented, corresponding SADP from an individual two-phase particle containing small amounts of α phase (dark) on opposite sides of the particle. The particle is near a $[112]$ zone-axis orientation and the rectangular arrangement of fundamental reflections corresponding to the Ag-rich phase is indicated in the SADP in Fig. 4(b). The strong reflections adjacent to the rectangular outline are from the Cu-rich majority phase while the weaker, inner reflections (outlined) are from the Ag-rich minority phase. This diffraction pattern shows that the two phases have a cube-on-cube (or parallel) orientation relationship (OR) [5,19]. This was usually the case, although occasionally the phases were observed to have a twin-related OR [20]. The extra spots in the SADP that are not included in either of the rectangular patterns are due to the stacking faults/twins seen in the Cu-rich β phase in Fig. 4(a). The $11\bar{1}$ reciprocal-lattice vector indicated on the BF image in Fig. 4(a) is normal to the approximately edge-on α/β interface in the lower-right corner, demonstrating that it is a $(11\bar{1})$ interface. The very small α phase in the upper-left corner appears to have an interface that is slightly inclined from $(11\bar{1})$. This might be due to the somewhat irregular shape of this particular two-phase par-

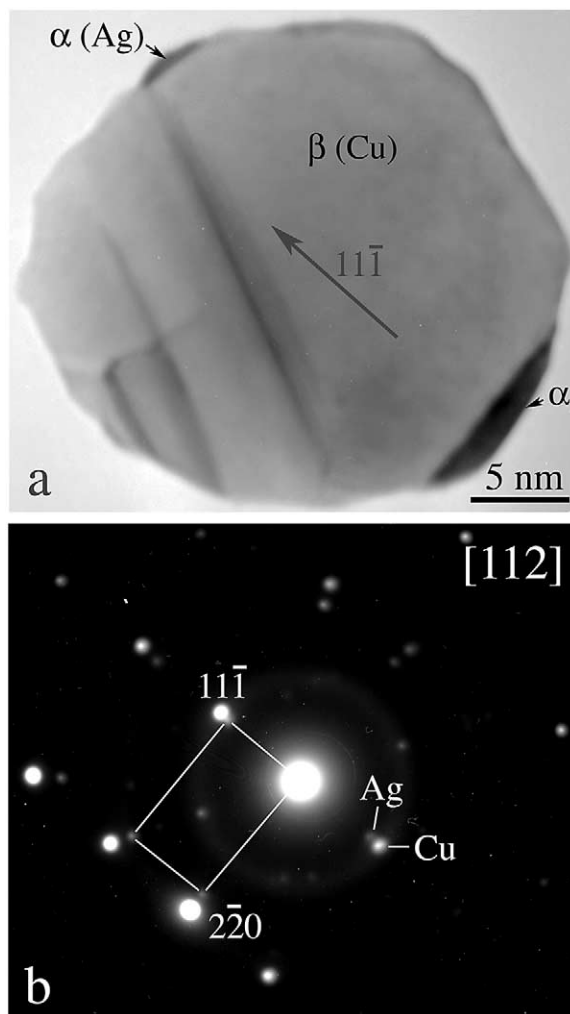


Fig. 4. (a) BF TEM image and (b) corresponding SADP from an individual two-phase nanoparticle containing small amounts of α phase (dark) on opposite sides of the particle.

ticle, which was atypical of most particles, but nevertheless, observed. Interfaces were occasionally found to deviate slightly from $\{111\}$ in other particles, but the majority of the α/β interfaces were parallel to $\{111\}$.

The relative difference in lattice parameters between the α and β phases of the particle shown in Fig. 4 was measured using an average value obtained from all of the well-separated spots in the SADP and yielded a value of $12.1 \pm 0.2\%$, somewhat less than the calculated value of 13.0% based on the lattice parameters of pure Ag and Cu, or the

value obtained by averaging over many particles in the ring pattern in Fig. 3(b). This difference is not unexpected as the ring patterns in Fig. 3(b) represent an average spacing obtained over many single-phase particles as well as over many two-phase particles with some mutual solubility in both phases. (The relative volume fractions of the single-phase and two-phase particles were not measured.) The small, single-phase particles are relatively pure and their lattice parameter should be comparable to their bulk values, neglecting surface-stress effects. As shown in subsequent EDXS analysis, the α and β phases in two-phase particles each contain several percent of the other element. Assuming a linear dependence of the lattice parameter on composition for both the α and β phases gives for the lattice parameter:

$$a = x(0.40857 \text{ nm}) + (1-x)(0.31647 \text{ nm}), \quad (15)$$

where x is the atomic fraction of Ag in the appropriate phase, and 0.40857 and 0.31647 nm are the lattice parameters of pure Ag and Cu, respectively. Using the values obtained from the EDXS data (in Section 4.2): $x = 0.962$ for the Ag-rich phase and $x = 0.034$ for the Cu-rich phase, the calculated relative difference in the lattice parameters is 12.0%, which is equal to the experimentally measured lattice parameter difference within the measurement error. These results are consistent with the following EDXS analyses and indicate that the relative difference in lattice parameters for the two-phase particles is approximately 1% less than the difference indicated from the ring patterns averaged over a mixture of single-phase and two-phase particles.

4.2. Energy-dispersive X-ray spectroscopy

Fig. 5(c) and (d) shows typical EDXS spectra obtained from the α and β phases in the two-phase particle shown in Fig. 5(a), as well as a spectrum (Fig. 5(b)) obtained by spreading the electron beam over the entire particle. The α and β phases are clearly Ag-rich and Cu-rich, containing approximately 96.2 and 3.4 at.% Ag, respectively, while the average composition of the entire particle was 44.0 at.% Ag. This result was typical for a number of such particles analyzed. It is important to note

that the overall composition of the alloy particles, obtained by spreading the beam over hundreds of particles at low magnification and acquiring an EDXS spectrum, was Cu–33.8 at.% Ag. The average compositions of individual particles varied considerably about this mean, from nearly pure Ag or Cu for the small particles, to between about 15–50 at.% Ag for the two-phase particles, with a few exceptions. A 0.5 nm diameter electron probe was placed on the surfaces of the α and β phases on the outer most edges from the α/β interface to look for evidence of Ag or Cu enrichment, i.e. surface segregation, but no obvious differences were seen compared to the average phase compositions.

According to the equilibrium Ag–Cu phase diagram [14], the solubility of Cu in the Ag-rich α phase is 3.5 and 0.3 at.% at 520 and 200 °C, respectively, while the solubility of Ag in the Cu-rich β phase is 0.93 and less than 0.06 at.% at 520 and 200 °C, respectively. Both phases have little solubility at room temperature. The compositions of the α and β phases obtained by EDXS analysis of the two-phase particles in the present study (shown in Fig. 5) revealed a significantly higher concentration of Ag present in the β phase (approximately 3.5 at.%) than that given by the equilibrium phase diagram, with approximately the same concentration of Cu present in the Ag-rich α phase (approximately 3.8 at.%) as given by the phase diagram. It is not likely that the higher than expected concentration of Ag in the β phase is due to an inaccurate k -factor used in quantification, or to adsorption and/or fluorescence of Ag or Cu X-rays given the large composition deviation in only one phase and the small size (~50 nm) of the two-phase particles analyzed. Hence, it appears that the Cu-rich β phase may have a higher solubility for Ag in these two-phase nanoparticles than indicated by the equilibrium Ag–Cu phase diagram. Such increases have been previously reported for other two-phase nanoparticles such as Bi–Sn, In–Sn [21] and Pt–Rh [22], although for significantly smaller particle sizes. It is also worth noting that the average composition measured for the Ag-rich α phase is similar to that given by the phase diagram at 520 °C and not to the phase diagram value at room temperature, indicating that either the particles cooled fast enough in vacuum after annealing that

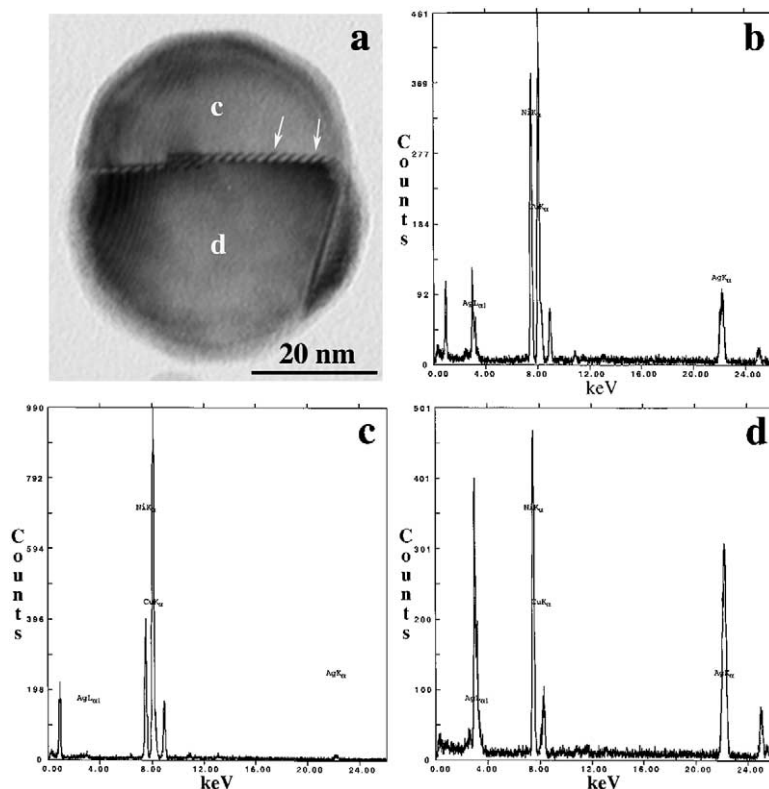


Fig. 5. (a) BF TEM image of a two-phase particle and EDXS spectra obtained by (b) spreading the beam over the entire particle, and (c, d) focusing the probe on the β and α phases, respectively.

significant solute partitioning did not occur, or that the α phase also has a higher solubility in these small two-phase particles, similar to the β phase.

The α/β interface in the two-phase particles in the size range 40–100 nm diameter appeared to be partly coherent, as previously observed for the interface between Ag precipitates in a Cu-rich matrix [19,20]. The dark lines, indicated by arrows in Fig. 5(a), are indicative of this effect. These lines, which are spaced about 1.6 nm apart, may arise from one set of misfit dislocations that is in contrast under the present diffraction conditions at the α/β interface, which is slightly inclined in this figure. However, the lines may also be a Moire pattern at the interface due to the lattice parameter difference and overlapping phases at the inclined interface [11]. A complete diffraction contrast analysis was not performed to distinguish between these two cases, but both are indicative of the high

misfit at, and partly coherent nature of, the α/β interface. The narrow width of the dark lines and their bending near the top and bottom surfaces of the particle in Fig. 5(a) are more characteristic of contrast that arises from dislocations than from Moire fringes, but more two-beam diffracting conditions are needed to distinguish unequivocally between these two possibilities.

4.3. Tri-junctions and dihedral angle measurements

Fig. 6 shows a BF TEM image of a typical two-phase particle used to measure the three dihedral angles, θ_α , θ_β and θ_v , at the tri-junction. In this image, the $\{111\}$ α/β interface is approximately edge-on and the tri-junctions are clearly visible. The surfaces of the α and β phases at opposite ends of the particles display $\{111\}$ facets parallel to the

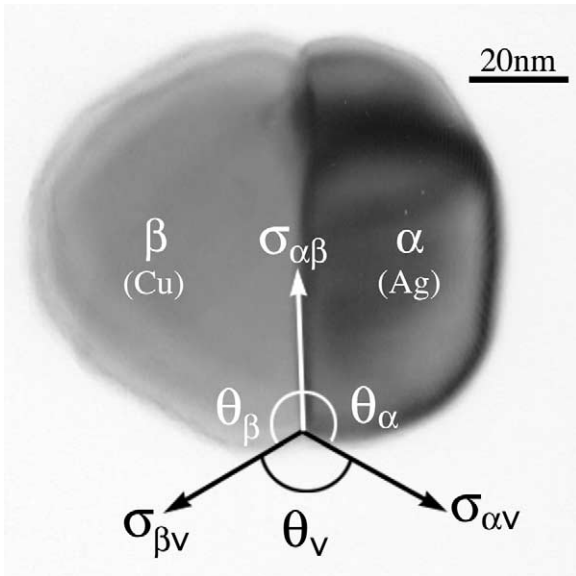


Fig. 6. BF TEM image of a typical two-phase nanoparticle used to measure the dihedral angles, θ_α , θ_β and θ_v , at the tri-junction. The $\{111\}$ α/β interface is approximately edge-on in this particle.

α/β interface. Distinct facets are not evident on the surfaces of the phases at the tri-junction in this particular particle, but this was not always the case, as shown in the next figure and discussed in more detail later.

Fig. 7 shows an HRTEM image of a tri-junction.

The Ag-rich α phase on the right is near a $\langle 110 \rangle$ zone-axis and the $\{111\}$ and $\{200\}$ planes are clearly visible, particularly near the tri-junction. The β phase on the left does not diffract as strongly, but two sets of $\{111\}$ planes are still visible. This particular image was acquired near the end of the study and some oxidation, particularly of the Cu-rich β phase (arrow), is evident on the particle surfaces. Nevertheless, the HRTEM image clearly reveals the atomic structure at the tri-junction, providing more detail than the conventional TEM images in Figs. 5(a) and 6. This particular tri-junction is somewhat unusual because the presence of several stacking faults in the α phase (labeled A) have caused the α/β interface at the bottom of the figure, which is parallel to a $\{111\}$ plane in the β phase (labeled B), to change orientation and lie along the $\{200\}$ plane in the α phase as it forms the tri-junction. In addition, the α/β interface at B is parallel to a $\{111\}$ plane in the β phase, but this phase is not in a $\langle 110 \rangle$ zone-axis orientation, indicating that the two-phase particle deviates from the exact cube-on-cube OR frequently observed. In spite of these irregularities, the α/β interface is still planar at the tri-junction and the dihedral angles are clearly visible. Notice that the α phase displays a $\{110\}$ facet adjacent to the tri-junction. This feature is discussed in more detail with reference to Fig. 11.

The dihedral angles at opposite ends of the α/β

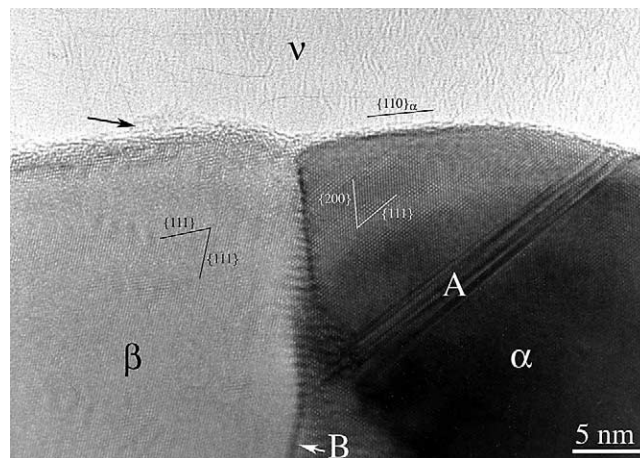


Fig. 7. High-resolution TEM image of a tri-junction with the Ag-rich α phase on the right and the Cu-rich β phase on the left. The α/β interface is approximately edge-on at the tri-junction and nearly parallels a $\{200\}$ plane in the α phase.

interface were measured for 12 different two-phase particles and plotted as a function of the α phase fraction P_f^α , as shown in Fig. 8. Most of the particles had phase fractions in the range of $0.15 < P_f^\alpha < 0.50$, although one particle was measured with $P_f^\alpha \approx 0.8$. Power-law curves were best-fit through the data, as shown by the solid lines in Fig. 8. Although there are considerable scatter in the data (the reason for this is discussed in Section 6), it is evident that there is a steady increase in θ_α from about 80–125° with increasing phase fraction α from 0.15 to 0.85. This is accompanied by a steady decrease in θ_β from approximately 120 to 85° and a gradual decrease in θ_v from about 165 to 155° over the same range of phase fraction α .

Fig. 9 shows a graph of $\cos \theta_\beta$ versus $\cos \theta_\alpha$ for the same measured dihedral angles plotted in Fig. 8. The linear fit through the data obtained by orthogonal regression analysis is indicated by the solid line in Fig. 9. The slope of this line, which from Eq. (12) yields the ratio of the surface energy densities of the α and β phases, $-\sigma_{\alpha v}/\sigma_{\beta v}$, was -0.61 , and the intercept with the vertical axis, which yields the ratio of the α/β interfacial energy to that of the β phase, $-\sigma_{\alpha\beta}/\sigma_{\beta v}$, was -0.29 . These ratios of the surface and interfacial energies were used for the particle calculations described in the next section. Alternatively expressed, the ratios of the surface energies of the Ag-rich and Cu-rich phases, $\sigma_{\alpha v}$ and $\sigma_{\beta v}$, to the interfacial energy, $\sigma_{\alpha\beta}$, were measured as 2.1 and 3.5, respectively.

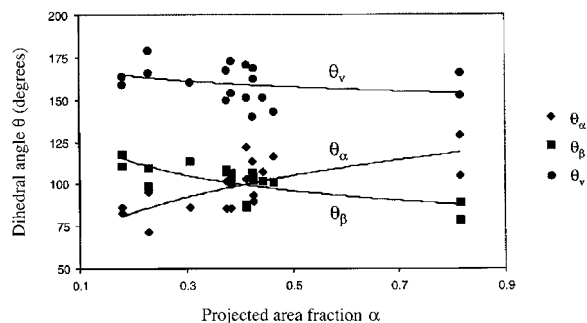


Fig. 8. Dihedral angles, θ , plotted as a function of the α phase fraction, P_f^α , for twelve different two-phase nanoparticles, with power-law fits through the data indicated by solid lines.

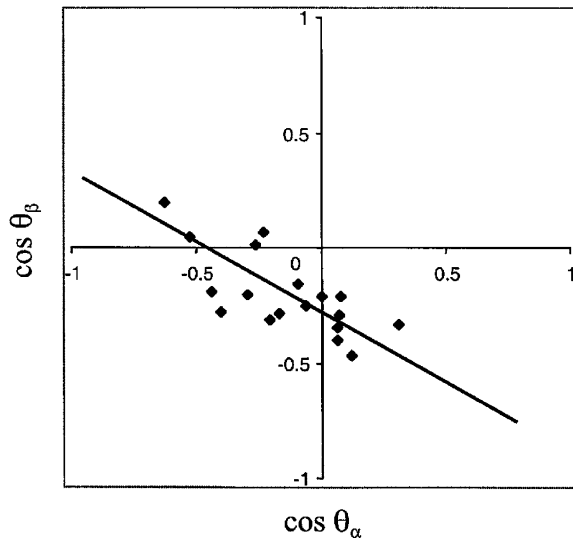


Fig. 9. Graph of $\cos \theta_\beta$ versus $\cos \theta_\alpha$ for the same dihedral angles plotted in Fig. 8, with a linear fit through the data indicated by the solid line.

5. Calculated shapes of two-phase particles

Fig. 10(a)–(c) shows the equilibrium particle shapes as calculated from Eq. (14) for three-phase-fractions of α , $P_f^\alpha = 0.17, 0.28$ and 0.44 . These figures were determined using the measured ratios

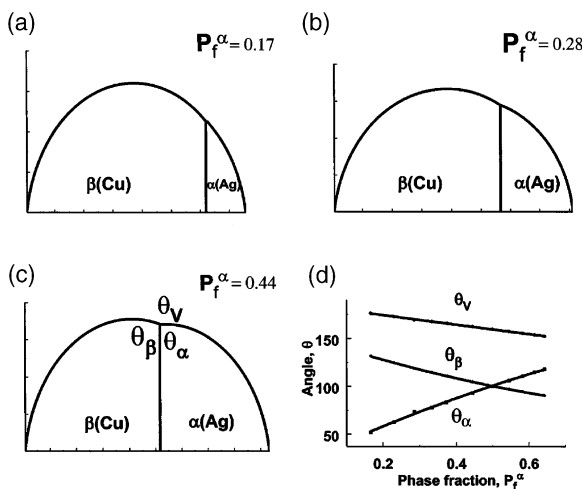


Fig. 10. (a)–(c) Equilibrium particle shapes calculated from Eq. (14) for α phase-fractions $P_f^\alpha = 0.17, 0.28$ and 0.44 , respectively, and (d) graph of the dihedral angles for these and other particles over the range of phase-fraction α from 0.15–0.7.

of the interfacial energies: $\sigma_{\alpha\beta}/\sigma_{\beta\nu} = 0.29$ and $\sigma_{\alpha\nu}/\sigma_{\beta\nu} = 0.61$. Fig. 10(d) shows a graph of the corresponding dihedral angles for these and other particles over the range of 0.15–0.7 phase fraction α . The graph in Fig. 9(d) can be compared directly with the experimental data shown in Fig. 8. This comparison shows similar trends in the behavior of the three angles at the tri-junction. Namely, that θ_{α} steadily increases with increasing phase fraction of α over the range shown, while θ_{β} steadily decreases and θ_{ν} gradually decreases over the same range of phase fraction α . Notice that the plots of θ_{α} and θ_{β} cross at approximately 0.5 phase fraction α in both Figs. 8 and 10(d), further indicating good qualitative agreement. The main difference between the experimental data in Fig. 8 and the calculated results in Fig. 10(d) is that the values for the dihedral angle θ_{α} in the modeling are about 25° lower than those determined experimentally and this is balanced by 10 – 15° increases in θ_{β} and θ_{ν} . Otherwise, there is a good overall agreement between the calculated and experimentally determined dihedral angles within the limited number of data points and scatter in the experimental data. If there were no dependence of the dihedral angles on the phase fractions, the graph in Fig. 10(d) would consist of three horizontal lines with the values of θ_{α} , θ_{β} and θ_{ν} determined from the values of the surface and interfacial energies using Eqs. (1) and (4).

There are many different combinations of surface and/or interfacial energies that can be used to demonstrate the various possible particle shapes and dihedral angles that result for two-phase particles. Only a few qualitative trends that have been observed based on initial calculations are described below. More quantitative results are being determined and will be published elsewhere [23]. As might be expected, it has been observed that increasing the interfacial energy relative to the two surface energies causes the particle to decrease the area of the α/β interface, thereby increasing the degree of puckering at the three-phase junction. This leads to smaller values of θ_{ν} and larger values of θ_{α} and θ_{β} . Conversely, decreasing the interfacial energy increases the interfacial area, causing the particle to become more spherical, with the angles adjusting accordingly. In the limiting case where

the interfacial energy approaches zero and the α and β phases have equal surface energies and phase fractions, the two-phase particle becomes spherical. These variations can cause θ_{ν} to lie above or below θ_{α} and θ_{β} on a plot such as Fig. 10(d), depending on the ratios of the surface energies to the interfacial energy.

6. Discussion

The TEM observations and equilibrium calculations demonstrate that the dihedral angles at a three-phase junction vary with the volume fraction of the phases for spherical two-phase particles, when one interface (in this case the α/β interface) is cusp-oriented. In the absence of a cusp-oriented interface, the dihedral angles of a tri-junction are uniquely determined if the tri-junction is in thermodynamic equilibrium. If the surface and interfacial energy densities are independent of the normal, the various isotropic surfaces will possess constant, but different, curvatures at equilibrium depending on the relative amounts of the phases present. When one interface becomes cusp-oriented, there exists only one equilibrium condition at the tri-junction and a degree of freedom is introduced in the selection of the dihedral angles. The equilibrium boundary condition at the tri-junction is coupled to the equilibrium condition for each of the surfaces (the Euler–Lagrange equations), as seen from Eq. (9). In this case, the boundary conditions must be satisfied or solved simultaneously with the equations determining the shapes of the surfaces. Since the shape of the surfaces depends on the relative amounts of the phases, it is to be expected that the dihedral angles will also show a dependence on the phase fraction.

A similar dependence of two of the dihedral angles on phase fraction should also exist when there are two cusp-oriented interfaces present in the tri-junction. This situation was observed for some particles, such as those appearing in Fig. 6 or Fig. 11. The two undetermined angles provide a degree of freedom that must be solved simultaneously with the equilibrium conditions for the surfaces; again suggesting a dependence of two dihedral angles on the phase fraction. The dihedral

angle determined by the two cusp-oriented surfaces is independent of phase fraction.

Part of the scatter in the data appearing in Fig. 8 is due to some particles forming with tri-junctions that possess two cusp-oriented interfaces. There is a tendency for the two-phase particles to facet along low-energy $\{111\}$, $\{200\}$ and other relatively low-index $\{hkl\}$ planes. Although the difference in the actual values of the surface energies of the $\{hkl\}$ planes for Cu and Ag might only vary by a few percent [24,25], this difference is sufficient to produce well-developed surface facets on the phases. Such facets were observed previously, for example in Fig. 6.

Fig. 11 shows how such faceting can affect the resulting dihedral angles measured at a three-phase junction. In this case, the α phase displays well-developed facets at both tri-junctions, but the orientations of the facets differ by almost 20° relative to the $\{111\}$ α/β interface, as indicated in the figure. This occurs because the facets are different $\{hkl\}$ planes, which produce different dihedral angles. In fact, this particle yielded the set of data for the phase fraction of approximately 0.8 in Fig. 8, where it is evident that the two data points for θ_α (diamonds) differ by about 20° , as in Fig. 11. If the particle in Fig. 11 were rotated about the $\{111\}$ interface-plane normal, the degree of faceting at the tri-junctions and the measured dihedral angles would vary. Clearly it would be of interest to measure and understand the dependence of the dihedral angles on the $\{hkl\}$ planes present in the α and β phases at the tri-junctions, although currently, we have insufficient data to do this.

In spite of the large variation in dihedral angles that faceting causes, the variations appear to average out when plotted as in Fig. 9, yielding reasonable average results for the surface and interfacial energies. That these results are reasonable is indicated by comparison of the experimentally determined ratio of the surface energies of Ag to Cu of 0.61, with a ratio of 0.68 based on the average surface energies of pure Ag and Cu, which are 1250 and 1850 mJ/m², respectively, at 0 K [5,13]. Similarly, the experimental ratio of the interfacial energy to the surface energy of the Cu phase of 0.29 yields a value of 537 mJ/m², based on the average surface energy of pure Cu at 0 K. This is

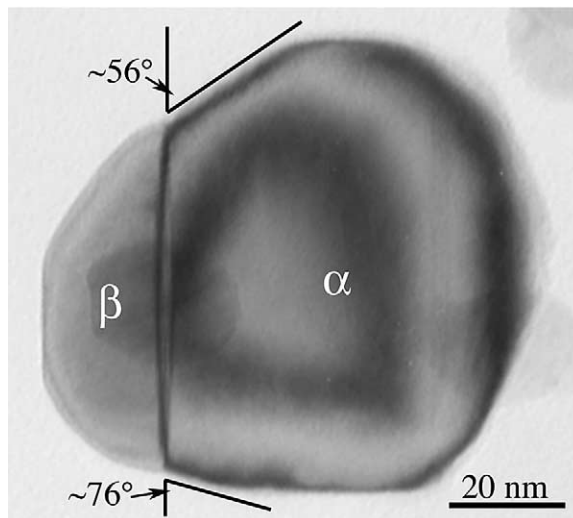


Fig. 11. BF TEM image of a two-phase particle where the α phase displays well-developed facets at both tri-junctions, but the orientations of the facets differ relative to the $\{111\}$ α/β interface.

a reasonable value for a partly coherent interface in fcc metals [5]. Faceting of the two-phase particles also affects comparison between the calculated and experimental measurements in another way. The area fractions measured experimentally are not those of perfectly spherical particles due to faceting. In contrast, the calculated phase fractions are always based on perfect spheres. This difference introduces some error between the measurements, but the error does not appear to be substantial.

It is also useful to compare the behavior of the current tri-junction configuration, where one interface is cusp-oriented, with other situations commonly encountered in materials science. Fig. 12(a)–(c) illustrates three common situations, Fig. 12(a) being the present case of one cusp-oriented interface. In this case, there are no surfaces or interfaces that are parallel, the orientation is fixed only for the α/β interface and the values of the dihedral angles θ_α , θ_β , and θ_v all depend on the phase fractions. The surfaces of both the α and β phases change orientation as the phase fractions change, as indicated by the arrows in the figure. The limits of the range of possible change are described in Ref. [8]. In addition to the two-phase

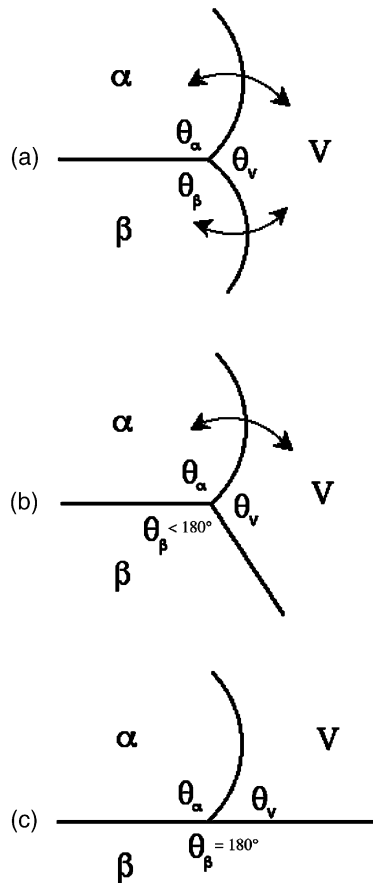


Fig. 12. Qualitative illustrations comparing the behavior of tri-junctions when: (a) one interface is cusp-oriented and (b,c) two interfaces are cusp-oriented, for situations commonly encountered in materials science.

particles in this study, this situation appears to be important in grain growth, where one grain-boundary is cusp-oriented, containing a $\{111\}$ twin boundary for example [6,8,26,27]. Its curvature and mobility may be markedly different from the other grain boundaries at the tri-junction, thereby affecting grain development. In Fig. 12(b), two interfaces are fixed in orientation, i.e. cusp-oriented, but not parallel. The β/v interface has been drawn straight in Fig. 12(b) for ease of comparison. In this case, the remaining α/v interface can vary its orientation and the angle θ_α increases with increasing fraction of α phase, as evident in the figure. This situation has been encountered in grain refining of molten Al alloys, where the orientation

and size of the β/v interface effectively limits the amount of interface available for nucleation of the α phase [28] and again, it may be important in grain growth [8,26]. The last situation in Fig. 12(c) is one of the most common configurations encountered in materials science. It is the classic 'sessile drop' experiment [2–5] with a liquid or solid drop on an effectively semi-infinite solid surface. In this case, the α/β and β/v interfaces coincide and are fixed in orientation. The angle θ_α does not vary with fraction of α phase, but the drop simply increases its size. In this case, there is no phase-fraction dependence and Eqs. (1) and (4) apply.

The behavior shown herein was for two metallic phases in equilibrium with their vapor, but similar behavior is expected to occur for other states and combinations of materials, as evidenced by the example of grain refining mentioned above. Certain factors such as a strong orientation dependence of the surface and interfacial energies may change the actual equilibrium angles quantitatively, but the same qualitative dependence on the phase fraction of material is anticipated.

7. Conclusions

The experimental observations and analytical calculations in this study support the following conclusions:

1. Small, two-phase particles of Ag–Cu alloys generally display a cube-on-cube OR with a $\{111\}$ partly coherent interface between the α and β phases, although variations on this behavior were sometimes observed. The particles sometimes display surface facets on $\{111\}$, $\{100\}$ as well as other planes and often contain stacking faults and twins on the $\{111\}$ planes.
2. The lattice parameter difference between the Ag-rich and Cu-rich phases in the two-phase particles was approximately $12.2 \pm 0.2\%$, or about 1% less than the value predicted for pure Ag and Cu phases. This result is consistent with EDXS analysis of the two phases, which showed that each contained several percent of the other element, thereby reducing the lattice parameter difference.

3. The dihedral angles of the three-phase junction formed by the two surfaces and the cusp-oriented {111} α/β interface are functions of the phase fraction.
4. The dependence of the tri-junction angles on phase fraction allows the ratios of the surface and interfacial energy densities to be determined experimentally using the tri-junction equilibrium conditions. In the Ag–Cu system, these ratios were determined as $\sigma_{\alpha v}/\sigma_{\beta v} = 0.61$ and $\sigma_{\alpha\beta}/\sigma_{\beta v} = 0.29$, respectively.
5. When surface facets are present at tri-junctions, as was frequently observed, the resulting dihedral angles can be altered, even for small values of surface anisotropy. This factor does not seem to lead to large variations in the measured ratios of the surface and interfacial energies due to data averaging.

Acknowledgements

The authors gratefully acknowledge Ms B. Huang and Mr T.C. Schamp for the help with the particle evaporations and Prof. W.A. Jesser for making this equipment available. The authors are also grateful to the National Science Foundation for support under Grants DMR-9902110 (WCJ, JMH, KC) and DMR-9900855 (JMH, PL, MM) and to the Fulbright Foundation (AMM).

References

- [1] Herring C. In: Kingston WE, editor. The physics of powder metallurgy. New York: McGraw-Hill, 1951. p. 143.
- [2] Young T. Philos Trans. R. Soc. Lond. 1805;95:65.
- [3] Adamson AW. Physical chemistry of surfaces, 2nd ed. New York: Wiley, 1967.
- [4] Murr LE. Interfacial Phenomena in Metals and Alloys. Reading, MA: Addison-Wesley, 1975. p. 3 [chapter 2].
- [5] Howe JM. Interfaces in materials: atomic structure, thermodynamics and kinetics of solid–vapor, solid–liquid and solid–solid interfaces. New York: Wiley, 1997. p. 176–83.
- [6] Hoffman DW, Cahn JW. Surf. Sci. 1972;31:368.
- [7] Cahn JW, Hoffman DW. Acta Metall. 1974;22:1205.
- [8] King AH. In: Weiland H, Adams BL, Rollett AD, editors. Grain growth in polycrystalline materials III. Warrendale: The Minerals, Metals and Materials Society, 1998. p. 333–8.
- [9] Uyeda R. J. Cryst. Growth 1974;24/25:69.
- [10] Romig Jr AD, Carr M. Thin Film Analysis, v.1.3—Report #SAND82-2938, Sandia National Laboratory, NM; 1989.
- [11] Fultz B, Howe JM. Transmission electron microscopy and diffractometry in materials science. Berlin: Springer, 2001.
- [12] Maddala GS. In: Econometrics. New York: McGraw-Hill, 1977. p. 294–6.
- [13] Alonso JH, March NH. In: Electrons in metals and alloys. London: Academic Press; 1989. p. 43–6.
- [14] Okamoto H, Massalski TB. Bull. Alloy Phase Diagrams 1983;4:30.
- [15] Hirth JP, Lothe J. Theory of dislocations. 2nd ed. New York: Wiley, 1982 [chapter 10].
- [16] Schmidt A, Schuenemann V, Anton R. Phys. Rev. B 1990;41:11875.
- [17] Kortekamp T, Anton R, Harsdorff M. Thin Solid Films 1986;145:123.
- [18] Barrett C, Massalski TB. Structure of metals. 3rd ed. Oxford: Pergamon Press, 1980 [Table A-6].
- [19] Rao G. A study of interphase boundary composition in metallic systems. PhD thesis, Carnegie Mellon University, 1994 [chapter 6].
- [20] Rao G, Howe JM, Wynblatt P. Scr. Metall. Mater. 1994;30:731.
- [21] Allen GL, Jesser WA. J. Cryst. Growth 1984;70:546.
- [22] Lyman CE, Lakis RE, Stenger Jr HG. Ultramicroscopy 1995;58:25.
- [23] Mebed AM, Johnson WC, Howe JM. In preparation.
- [24] McLean M. Acta Metall. 1971;19:387.
- [25] Heyraud JC, Metois JJ. Acta Metall. 1980;28:1789.
- [26] Koo JB, Yoon DY. Metall. Mater. Trans. 2001;32A:1911.
- [27] Lee SB, Yoon DY, Henry MF. Acta Mater. 2000;48:3071.
- [28] Greer AL, Bunn AM, Tronche A, Evans PV, Bristow DJ. Acta Mater. 2000;48:2823.